RESEARCH ARTICLE

Diet-derived ergothioneine induces necroptosis in colorectal cancer cells by activating the SIRT3/MLKL pathway

Nunzia D'Onofrio[1], Elisa Martino[1], Anna Balestrieri[2], Luigi Mele[3], Domenico Cautela[4], Domenico Castaldo[4,5] and Maria Luisa Balestrieri[1] (iD)

1 Department of Precision Medicine, University of Campania Luigi Vanvitelli, Naples, Italy
2 Department of Animal Health, Istituto Zooprofilattico Sperimentale del Mezzogiorno, Portici, Italy
3 Department of Experimental Medicine, University of Campania Luigi Vanvitelli, Naples, Italy
4 Stazione Sperimentale per le Industrie delle Essenze e dei Derivati dagli Agrumi (SSEA) – Azienda Speciale CCIAA di Reggio Calabria, Italy
5 Ministero dello Sviluppo Economico (MiSE), Rome, Italy

Correspondence
M. L. Balestrieri, Department of Precision Medicine, University of Campania Luigi Vanvitelli, Via L. De Crecchio 7, 80138 Naples, Italy
Tel.: +39 081 5665865
E-mail: marialuisa.balestrieri@unicampania.it

Ergothioneine (Egt) is a dietary amino acid which acts as an antioxidant to protect against ageing-related diseases. We investigated the anti-cancer properties of Egt in colorectal cancer cells (CRC). Egt treatment exerted cytotoxicity in a dose-dependent manner, induced reactive oxygen species accumulation, loss of mitochondrial membrane potential and upregulation of the histone deacetylase SIRT3. Immunoblotting analysis indicated that the cell death occurred *via* necroptosis through activation of the RIP1/RIP3/MLKL pathway. An immunoprecipitation assay unveiled that the interaction between the terminal effector in necroptotic signalling MLKL and SIRT3 increased during the Egt treatment. SIRT3 gene silencing blocked the upregulation of MLKL and abolished the ability of Egt to induce necroptosis. The SIRT3–MLKL interaction may mediate the necroptotic effects of Egt in CRC, suggesting the potential of this dietary amino thione in the prevention of CRC.

Keywords: colon cancer; ergothioneine; necroptosis; RIP1/RIP3/MLKL; SIRT3

Ergothioneine (Egt), the betaine of 2-mercapto-L-histidine, is a diet-derived amino acid with antioxidant properties occurring at particularly high levels in some foods including certain species of mushrooms, grains, black and red beans, red meat, liver and kidney [1,2]. Evidence from *in vitro*, animal models, and even clinical studies, has demonstrated that Egt is associated with reduced mortality and decreased risk of cardiovascular disease, as it possesses many properties, including cardioprotective and anti-diabetic effects [1–8]. The cytoprotective effects of Egt against cardiovascular diseases and chronic inflammatory conditions occur *via* modulation of the sirtuins SIRT1 and SIRT6 [9]. Additional evidence suggested that Egt targets mitochondria and could dampen the excess of mitochondria-specific reactive oxygen species (ROS) in response to oxidative stress [10]. Indeed, the organic cation transporter novel-type 1 (OCTN1), responsible for

Abbreviations
c-IAP1/2, cellular inhibitor of apoptosis 1 and 2; CRC, colorectal cancer; CYLD, cylindromatosis deubiquitinase; Egt, Ergothioneine; IL, interleukin; IP, immoprecitation; MDA, malondialdehyde; MLKL, mixed lineage kinase domain like; MMP, mitochondrial membrane potential; NAC, N-acetyl-L-cysteine; NEC1, necrostatin-1; RIP, receptor-interacting serine/threonine-protein kinase; ROS, reactive oxygen species; siRNA, small interfering RNA; SIRT3, sirtuin 3; TNF, tumour necrosis factor; USP22, ubiquitin-specific peptidase 22.

Egt uptake and accumulation in human tissues, is present at high expression levels in certain cells (blood cells, bone marrow, ocular tissues and brain) that are likely predisposed to oxidative stress [11,12]. Changes in expression and/or activity of carnitine transporters in plasma or intracellular membranes are expected, especially in cancers, including colorectal cancer (CRC), which are characterized by an altered fatty acid metabolism. Indeed, CRC cells express OCTN1 and OCTN2 transporters [13,14]. OCTN1 is associated with sporadic CRC in early age and its polymorphisms, L503F, is a biomarker of malignant progression of the disease [15]. Moreover, the polymorphism rs27437 of OCTN2, downregulating the OCTN2 expression, correlates with the increased CRC risk [16].

In cancer cells, preclinical studies showed that bioactive dietary compounds exert anti-tumour effects by inducing ROS-mediated cytotoxicity [17]. The redox imbalance displayed by cancer cells due to increased ROS levels promotes carcinogenesis by activating oncogenes and raising oxidative stress. This unique feature influences cancer cell proliferation, survival and apoptosis [17].

In CRC cells, the chemopreventive effects of a diet-derived betaine, δ-valerobetaine, is primed by altered redox homeostasis accompanied by upregulation of SIRT6, downregulation of SIRT3 and mitochondrial dysfunction [18,19]. In this context, other betaines occurring in commonly consumed foods could be active in the CRC chemoprevention, highlighting the importance of exploring their anti-cancer properties in the setting of targeted redox-modulating preventive strategies. Despite the numerous evidences on the cytoprotective and anti-inflammatory action of Egt, to date, there is no evidence that describes its potential in the modulation of the redox homeostasis in CRC, the third most common cancer worldwide in terms of incidence and second in terms of mortality, with 1.9 million cases and 935 000 deaths in 2020 [20].

Numerous studies have highlighted the crucial role of specific epigenetic enzymes in CRC pathogenesis, focusing on seven NAD^+-dependent class III histone deacetylases (HDACs), or sirtuins (SIRTs) [21]. Among sirtuins, the mitochondria guardian SIRT3 shuttles from the nucleus to the mitochondria where it acts on fatty acid β-oxidation, amino acid metabolism and tricarboxylic acid cycle [22,23]. The intriguing role of SIRT3 in CRC occurs by increasing ROS production and PINK1/Parkin/mitophagy axis activation and by mediating metabolic reprogramming *via* PPAR-α, PPAR-γ protein expression levels and apoptotic induction [19,24]. Necroptosis, a backup cell death mechanism, has emerged as a form of lytic programmed cell death, known to regulate cell death and to provoke the release of damage-associated molecular patterns into the extracellular space, thus resulting in a pro-inflammatory outcome [25]. The necroptotic signalling pathway, a caspase-8-independent cell death mechanism, is driven by the cytosolic necrosome complex consisting of receptor-interacting serine/threonine protein kinases (RIP)-1, RIP3 and the mixed lineage kinase domain-like (MLKL) pseudokinase [26–29]. In addition to MLKL, ROS represent the major effectors in necroptosis by RIP3, which increases mitochondrial ROS production through the activation of metabolism-related enzymes [30,31].

Recent studies have revealed a key role of necroptosis in tumorigenesis and metastasis, opening new perspectives on the potential of targeting necroptosis as a novel cancer therapy [32]. However, the precise role of MLKL, the terminal effector in necroptotic signalling and that of RIP3 in CRC tumorigenesis is not fully clarified. The present study aimed at investigating the anti-cancer properties of Egt in CRC, focusing on the interchanges of cell death mechanisms (necrosis and apoptosis), oxidative stress and inflammatory damage responses.

Materials and methods

Cell culture and treatment

Human colon epithelial CCD 841 CoN cells (CRL-1790) and human colorectal adenocarcinoma SW620 (CCL-227), HT-29 (HTB-38) and LoVo (CCL-229) cell lines were obtained from American Type Culture Collection (ATCC). CCD 841 CoN cells were grown in Eagle's minimum essential medium (EMEM, 30-2003, ATCC), while SW620 was maintained in Leibovitz's L-15 (L-15, 11415-064, Gibco, Thermo Scientific, Rockford, IL, USA), HT-29 in McCoy's 5A (16600-082, Gibco) and LoVo in F-12K medium (21127-002, Gibco). Cell culture medium was supplemented with 100 U·mL^{-1} penicillin, 100 mg·mL^{-1} streptomycin and 10% heat-inactivated fetal bovine serum (FBS, 10270106, Gibco). Cells were grown as a monolayer at 37 °C in a humidified atmosphere, with 5% CO_2, and the medium was changed two or three times per week. The day before treatment, cells were seeded into multi-well plates to allow attachment. Egt (sc-200814, Santa Cruz Biotechnology, Inc., Heidelberg, Germany) was dissolved in Hanks' balanced salt solution (HBSS)-10 mM Hepes. Treatments were performed by culturing cells in complete media with increasing Egt concentration (0.5–3 mM) for a maximum time of 72 h. Control cells (0 mM) were maintained in media containing the higher corresponding volume of HBSS-10 mM Hepes. The impacts of oxidative stress, apoptosis and necroptosis were assessed by pretreating cells for 1 h with 2 mM of the antioxidant N-acetyl-L-cysteine (NAC, A7250-25G, Sigma Aldrich, St. Louis, MO, USA) or with 50 μM necrostatin-1

(NEC1, T1847, TargetMol Chemicals, Wellesley Hills, MA), the receptor-interacting serine/threonine-protein kinase 1 (RIP1) inhibitor, commonly used to suppress necroptosis.

Viability assay

CCD 841 CoN, SW620, HT-29 and LoVo cells were seeded in 96-well plates at a density of 2×10^3 cells per well in the specific growth medium. After treatment, cell viability was detected using Cell Counting Kit-8 (CCK-8, Dojindo Molecular Technologies, Tokyo, Japan), as manufacturer's instruction reported. The assay is based on the highly water-soluble tetrazolium salt, WST-8, reduced by dehydrogenase activities in cells to give a yellow colour formazan dye, which is soluble in the tissue culture media. The amount of the formazan dye, generated by the activities of dehydrogenases in cells, is directly proportional to the number of living cells. In detail, CCK-8 solution (10 µL per well) was added and plates incubated at 37 °C for 4 h. Thereafter, absorbance was measured at 450 nm using a microplate reader model 680 (Bio-Rad, Segrate (MI) - Italy). All experiments were performed with $n = 4$ replicates.

Cell cycle study

SW620, HT-29 and LoVo cells were seeded in six-well plates at a density of 8×10^4/well for treatments. Cells were then trypsinized and stained for 1 h in the dark in a propidium iodide (PI) solution consisting of 50 µg·mL^{-1} PI, 0.1% sodium citrate, 25 µg·mL^{-1} RNase A and 0.1% Triton in phosphate-buffered saline (PBS). Flow cytometric evaluation was performed by collecting at least 20 000 events with a BD Accuri™ C6 (BD Biosciences, Milano, Italy) cytometer. Data analysis was performed with MODFIT LT V4.1.7 software (Verity Software House, Becton Dickinson, Topsham, ME, USA). Experiments were carried with $n = 3$ replicates.

Apoptotic and necrotic cell death evaluation

After treatment, SW620, HT-29 and LoVo cells were detached by trypsinization, washed with PBS and then apoptotic (Annexin V-FITC-positive, PI-positive) from necrotic (Annexin V-FITC-negative, PI-positive) cells distinguished by the Annexin V Apoptosis detection kit (556547, BD Pharmingen, Lyngby, Denmark), following manufacturer's instruction. Briefly, cells were re-suspended in 500 µL binding buffer 1X and incubated for 30 min with 2 µL Annexin V-FITC and 2 µL PI. Detection of viable, early or late apoptosis and necrotic cells was performed using a BD Accuri™ C6 (BD Biosciences) cytometer and data analysed by FLOWJO V10 software (Williamson Way, Ashland, OR, USA). For each sample, 20 000 events were recorded. Experiments were performed with $n = 4$ replicates.

Oxidative stress detection

Intracellular and mitochondrial content of reactive oxygen species (ROS) was evaluated, according to manufacturer's protocol, by using CellROX Green Reagent (C10444, Invitrogen, Waltham, MA, USA) and MitoSOX Red Mitochondrial Superoxide Indicator (M36008, Invitrogen). SW620, HT-29 and LoVo cells were seeded in six-well plates and, after 72 h Egt treatment, cells were stained by adding to the medium 5 µM CellROX or MitoSOX fluorogenic probes and incubating the plate at 37 °C for 30 min. After washing with PBS, CRC cells were imaged on a fluorescence microscope EVOS FL Cell Imaging System (Thermo Scientific, Rockford, IL, USA) and then intracellular and mitochondrial ROS fluorescence intensities quantified using a BD Accuri™ C6 cytometer (BD Biosciences). At least 20 000 events were recorded for each sample and cytometric analysis was performed with FLOWJO V10 software. Experiments were performed with $n = 3$ replicates. Menadione (100 µM) (M57405, Sigma Aldrich) was incubated for 1 h at 37 °C and used as ROS-positive control.

Extracellular ROS evaluation

The Amplex Red Hydrogen Peroxide/Peroxidase Assay kit (A22188, Invitrogen) was used to evaluate the extracellular H_2O_2 released in SW620, HT-29 and LoVo cells after 72 h treatment with Egt. Trypsinized cells were dispersed to produce a 20 µL cell suspension containing 2×10^4 live cells in Krebs-Ringer phosphate glucose buffer (145 mM NaCl, 5.7 mM sodium phosphate, 4.86 mM KCl, 0.54 mM CaCl$_2$, 1.22 mM MgSO$_4$, 5.5 mM glucose, pH7.35). Amplex red reagent (100 µL), containing 50 µM Amplex Red and 0.1 U HRP·mL^{-1}, was added to cells followed by 1 h incubation at 37 °C. Fluorescence of the oxidized product, 10-acetyl-3,7-dihydroxyphenoxazine, was measured with an Infinite 2000 Multiplate reader (Tecan, AG, Switzerland) using a 530 nm excitation wavelength and a 590 nm emission wavelength. The Egt autofluorescence value was subtracted to each sample measurement. H_2O_2 extracellular content was quantified using a standard curve (0–2 µM concentration range).

Assessment of mitochondrial membrane potential

JC-1 staining (MT09, Dojindo Molecular Technologies, Tokyo, Japan) was used according to the manufacturer's protocols to study mitochondrial membrane potential. SW620, HT-29 and LoVo cells were treated with Egt for 72 h and then stained with 5 µM JC-1 probe at 37 °C for 1 h in the dark. Subsequently, cells were detached and fluorescence detected with BD Accuri™ C6. Data were analysed with FLOWJO V10 software and at least 20 000 events were recorded for each sample.

Lipid peroxidation detection

Lipid peroxidation levels were assessed by measuring the cellular content of malondialdehyde (MDA) with colorimetric Lipid Peroxidation (MDA) Assay kit (ab118970, Abcam, Cambridge, UK), according to the manufacturer's instructions. In this protocol, the MDA in the sample reacts with thiobarbituric acid (TBA) to generate a MDA-TBA adduct, whose colorimetric quantification may be reported as MDA levels. In detail, after 72 h Egt treatment, SW620, HT-29 and LoVo cells were harvested and homogenized in 303 µL of MDA lysis solution. To generate MDA-thiobarbituric acid (TBA) adduct, 600 µL of TBA reagent was added to 200 µL of sample, and the mixture incubated at 95 °C for 60 min and then cooled in ice. Absorbance of the resulting supernatant, containing MDA-TBA adduct, was measured at 532 nm with a 680-microplate reader (Bio-Rad) and total MDA levels (nmol per mg of protein) were calculated comparing each sample absorbance to a standard curve and normalized to protein content.

SIRT3 silencing

SW620, HT-29 and LoVo cells were transfected with 40 nM small interfering RNA (siRNA, 438080910101, Applied Biological Materials, Richmond, BC, Canada), consisted of a mixture of three target sequences for human SIRT3 (1045: 5′–GCU UGA UGG ACC AGA CAA ATT UUU GUC UGG UCC AUC AAG CTT–3′; 772: 5′–CUU GCU GCA UGU GGU UGA UTT AUC AAC CAC AUG CAG CAA GTT–3′ and 410: 5′–CUC CCA UUC UUC UUU CAC AUU UGU GAA AGA AGA AUG GGA GTT–3′), and with 40 nM control non-targeting siRNA (NT-siRNA, 5′–UUC UCC GAA CGU GUC ACG UTT–3′ and 5′–ACG UGA CAC GUU CGG AGA ATT–3′) using the transfection reagent RNAifectin. Cells were seeded in six-well plate in complete culture medium. After 24 h, the growth medium was removed and cells were transfected with SIRT3 siRNA or NT-siRNA in serum- and antibiotic-free medium. Cells were incubated for 10 h, followed by additional 12 h of incubation after the addition of 10% FBS to each well. Transfected cells were then treated with 2 mM Egt for 72 h.

Cell lysis and immunoblotting analysis

After 72 h Egt treatment, SW620, HT-29 and LoVo cells were lysed with RIPA lysis buffer (1% NP-40, 0.5% sodium deoxycholate and 0.1% SDS in PBS) containing 10 µg·mL^{-1} aprotinin, leupeptin and 1 mM phenylmethylsulfonyl fluoride. Cell lysates were incubated for 1 h on ice and centrifuged at 10 000 g for 20 min at 4 °C. Protein samples (20–40 µg) were separated by SDS-PAGE and transferred to nitrocellulose membranes (Bio-Rad). Non-specific binding sites were blocked for 1 h at room temperature (RT) in 1× TBS 1% casein blocker (1610782, Bio-Rad). Membranes were then incubated at 4 °C overnight with specific primary antibodies: anti-SIRT3

(1 : 2000, PA5-86035, Invitrogen), anti-SIRT1 (1 : 1000, ab110304, Abcam), anti-SIRT6 (1 : 2000, ab191385, Abcam), anti-acetylated p53 (1 : 1000, ab75754, Abcam), anti-caspase-3 (1 : 1000, 9662, Cell Signaling Technology), anti-caspase-9 (1 : 1000, 9508, Cell Signaling Technology), anti-caspase-8 (1 : 1000, ab108333), anti-cellular inhibitor of apoptosis 1 and 2 (c-IAP1/2, 1 : 1000, sc-12410, Santa Cruz), anti-cylindromatosis deubiquitinase (CYLD, 1 : 1000, 8462, Cell Signaling Technology), anti-mixed lineage domain-like protein (MLKL, 1 : 1000, ab196436, Abcam), anti-receptor-interacting protein 1 (RIPK1/RIP1, 1 : 1000, SAB3500420, Sigma-Aldrich), anti-RIPK3/RIP3 (1 : 1000, NBP1-77299, Novus Biologicals, Milano, Italy), anti-ubiquitin-specific peptidase 22 (USP22, 1 : 1000, sc-390585, Santa Cruz), anti-tumour necrosis factor alpha (TNF-α, 1 : 1000, ab6671, Abcam), anti-nuclear factor kappa B (NF-κB, 1 : 1000, C22B4, Cell Signaling Technology), anti-interleukin-6 (IL-6, ab229381, 1 : 1000, Abcam), anti-cyclin B1 (1 : 1000, 4138, Cell Signaling Technology), anti-cyclin D1 (1 : 1000, ab134175, Abcam), anti-α-tubulin (1 : 5000, E-AB-20036, Elabscience Biotechnology Inc., Houston, TX, USA), anti-β-actin (1 : 5000, ab8227, Abcam) and anti-glyceraldehyde-3-phosphate dehydrogenase (GAPDH, 1 : 2000, ab9485, Abcam). After 1 h incubation with HRP-conjugated secondary antibodies (GxMu-003-DHRPX and GtxRb-003-DHRPX, ImmunoReagents Inc., Raleigh, NC, USA), the immunocomplexes were revealed on dried membranes by Excellent Chemiluminescent Substrate kit (E-IR-R301, Elabscience Biotechnology Inc.) and visualized by using ChemiDoc Imaging System with IMAGE LAB 6.0.1 software (Bio-Rad Laboratories). After background subtraction, the densities of immunoreactive bands were quantified with IMAGEJ software (Wayne Rasband, National Institutes of Health, USA) and expressed as arbitrary units (AU).

Immunoprecipitation assay

Immunoprecipitation (IP) was performed on 200 µg of total protein content using Immunoprecipitation kit (ab206996, Abcam) based on Protein A/G Sepharose® beads. Protein lysate was firstly incubated overnight with 2 µg MLKL antibody at 4 °C with shaking. The next day, the Protein A/G Sepharose® beads were introduced into the mixture and shaken for additional 3 h at 4 °C. Samples were then washed three times and elution was obtained by heating mixture at 95 °C for 15 min in loading buffer (4×) before separation by SDS-PAGE. After nitrocellulose membrane transfer and non-specific binding sites blocking, immunoblotting for SIRT3 was performed in order to determine the amount of MLKL/SIRT3 immunoprecipitated.

Statistical analysis

All reported data are expressed as mean ± standard deviation (SD) of experiments performed in at least three replicates. Statistical analysis between two groups was carried using Student's t test while differences among three groups were evaluated by

one-way ANOVA followed by Tukey *post hoc* test. Differences with $P < 0.05$ were considered statistically significant.

Results

Egt induced a selective inhibition of CRC cell viability

Egt (0–3 mM) was tested in human CRC SW620, HT-29 and LoVo cell and in colon CCD 841 CoN cells

(Fig. 1, Fig. S1). Cell viability assay showed that Egt (2 mM) displayed the higher cytotoxic effect on CRC cell lines reaching a cell viability inhibition of $40.7 \pm 5.47\%$ in HT-29, $41.5 \pm 4.22\%$ in SW620 and $38.8 \pm 6.1\%$ in LoVo cells after 72 h of treatment ($P < 0.001$) (Fig. 1A–C, Fig. S1C–E). A similar trend was observed using Egt 2.5 and 3 mM. Conversely, Egt treatment up to 72 h did not induce inhibition of cell viability in normal CCD 841 CoN (Fig. S1A,B). Based on these results, further experiments were performed
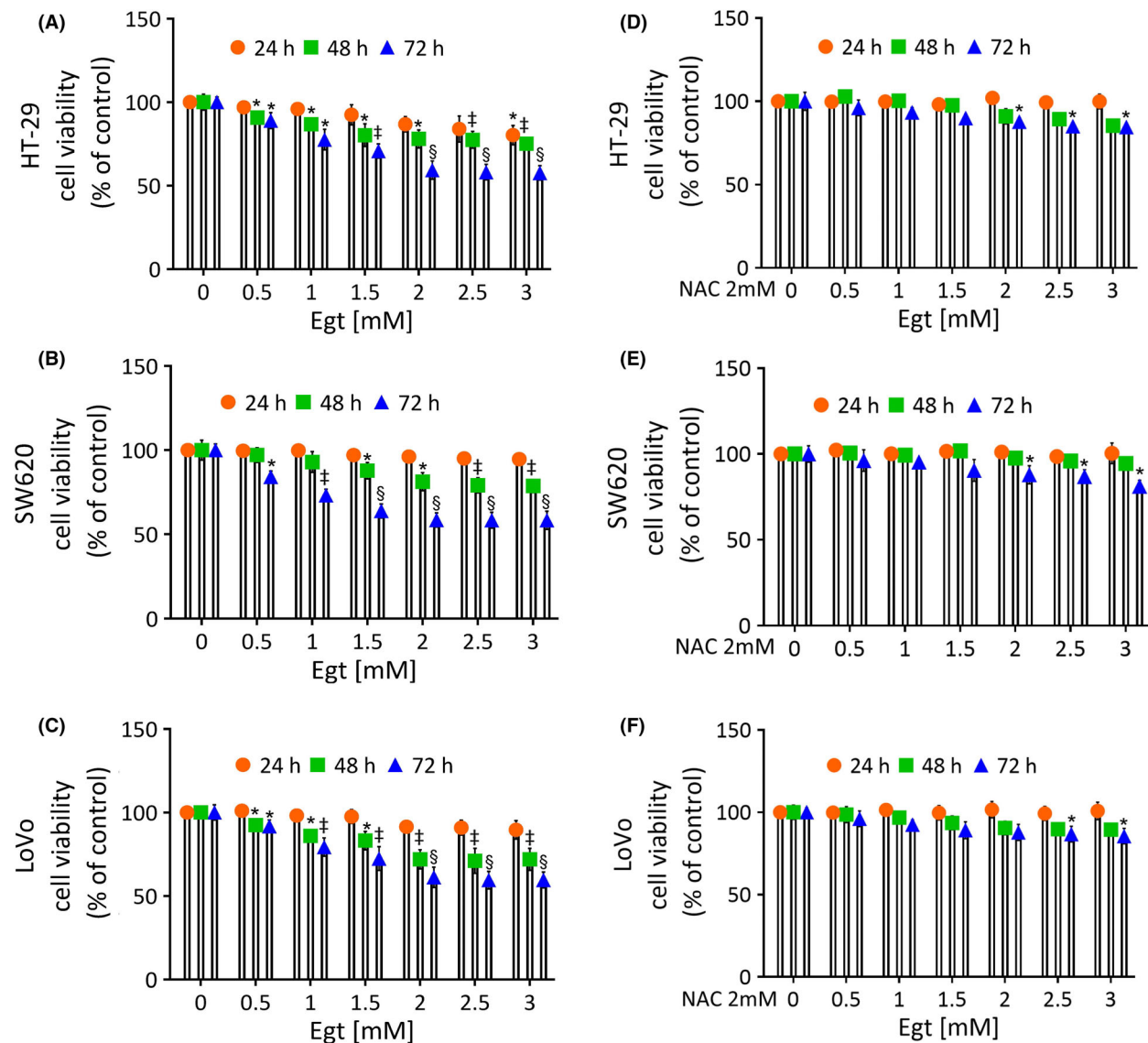

Fig. 1. Egt inhibited CRC cell viability. Cell viability was evaluated in (A) HT-29, (B) SW620 and (C) LoVo cell lines after exposure to different Egt concentration (0, 0.5, 1, 1.5, 2, 2.5 and 3 mM) for different times (24, 48 and 72 h). (D) HT-29, (E) SW620 and (F) LoVo cells were pretreated with 2 mM NAC for 1 h before exposure to increasing Egt concentrations up to 72 h and then viability assessed using Cell Counting Kit-8 assay (Donjindo Molecular Technologies). Control cells (0 mM) were grown in medium containing the higher corresponding volume of HBSS-10 mM Hepes. Values represent the mean $\pm$ SD of $n = 4$ independent experiments and results expressed as percentage of control. $*P < 0.05$ vs. 0 mM; $\ddagger P < 0.01$ vs. 0 mM; $\S P < 0.001$ vs. 0 mM.

choosing 1, 1.5 and 2 mM Egt concentration. Moreover, N-acetyl-L-cysteine (NAC) treatment before exposure to Egt, strongly attenuated the Egt-mediated cytotoxicity ($P < 0.05$) (Fig. 1D–F), suggesting that CRC cell damage induced by Egt occurs *via* oxidative stress.

Egt generated oxidative stress at different cellular levels

To shed light on the Egt-mediated cytotoxicity, the oxidative stress was assessed in CCD 841 CoN, SW620, HT-29 and LoVo cells. Results indicated the Egt capability to modulate intracellular, mitochondrial and extracellular ROS content, along with modification in the mitochondrial membrane potential (MMP) state (Fig. 2). Indeed, Egt treatment induced a strong

increase ($P < 0.01$) in fluorescent signal of intracellular and mitochondrial oxygen species in SW620 cells (Fig. 2A,B and Fig. S2A–C). These effects were also accompanied by the Egt-mediated upregulation in extracellular ROS content (368.4 ± 12.9 Egt 2 mM vs. 150.8 ± 8.8 of 0 mM, $P < 0.001$) and by the impairment of MMP (Fig. 2C–E), as revealed by the green fluorescence accumulation proper of monomeric species of JC-1 probe ($P < 0.01$). Similar results were detected in HT-29 cells with intracellular and mitochondrial enhancement of superoxide species ($P < 0.01$), extracellular ROS production (342.0 ± 21.1 Egt 2 mM vs. 103.7 ± 18.9 of 0 mM, $P < 0.001$) and perturbation in mitochondrial potential ($P < 0.01$) (Fig. 2F–J and Fig. S2D–F). In LoVo cells, Egt also provoked intracellular and mitochondrial ROS accumulation ($P < 0.001$), extracellular reactive species
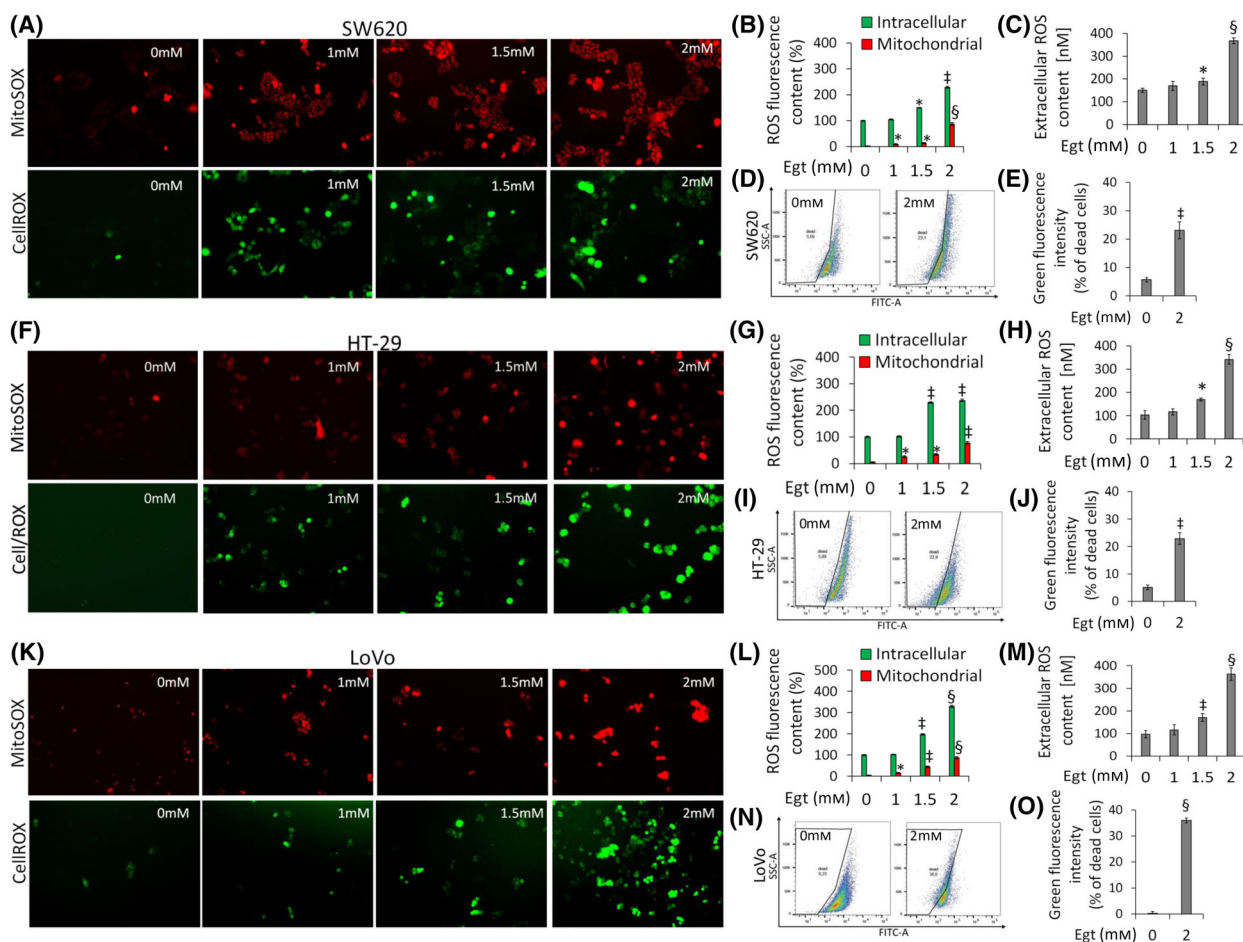

Fig. 2. Egt induced oxidative stress in CRC cells. Representative images and analysis of intracellular and mitochondrial superoxide levels, extracellular H_2O_2 production and mitochondrial membrane potential assessed in (A–E) SW620, (F–J) HT-29 and (K–O) LoVo cells treated for 72 h with Egt. Control cells (0 mM) were grown in medium containing the higher corresponding volume of HBSS-10 mM Hepes. Magnification: 20×. Data are shown as mean ± SD of $n = 3$ independent experiments. $^*P < 0.05$ vs. 0 mM; $^‡P < 0.01$ vs. 0 mM; $^§P < 0.001$ vs. 0 mM.

upregulation (362.7 ± 27.5 Egt 2 mM vs. 96.4 ± 15.9 of 0 mM, $P < 0.001$) and mitochondrial depolarization ($P < 0.001$) (Fig. 2K–O and Fig. S2G–I). Conversely, no effects were observed in oxidative state of CCD 841 CoN after Egt treatment (Fig. S2J–M). Finally, the pretreatment with the antioxidant NAC (2 mM), able to scavenge ROS levels, opposed the pro-oxidant action of Egt (Fig. S3).

Egt triggered pro-inflammatory milieu and upregulated sirtuins

The cytotoxicity of Egt on CRC cells was accompanied by its efficacy in modulating lipid peroxidation, inflammation and SIRT3 protein expression. In SW620 cells, Egt treatment for 72 h induced oxidative inflammation in a dose-dependent manner ($P < 0.01$), promoting upregulation of TNF-α (1.15 ± 0.05 AU vs. 0.53 ± 0.04 in 0 mM), IL-6 (1.88 ± 0.06 AU vs.

0.77 ± 0.03 in 0 mM) and NF-κB (1.10 ± 0.05 AU vs. 0.57 ± 0.04 in 0 mM) protein expression levels ($P < 0.001$) (Fig. 3A–D). These pro-inflammatory effects were accompanied by an increase in the SIRT3 protein content (1.14 ± 0.02 AU vs. 0.33 ± 0.04 in 0 mM, $P < 0.001$) (Fig. 3E). Egt displayed similar effects in HT-29 cells, leading to lipid peroxidation ($P < 0.01$), increase in TNF-α, IL-6 and NF-κB protein expression ($P < 0.001$), and SIRT3 protein (0.83 ± 0.025 AU vs. 0.28 ± 0.03 in 0mM, $P < 0.001$) (Fig. 3F–J). Egt treatment was effective in triggering oxidative damage ($P < 0.01$), increasing inflammatory protein content ($P < 0.001$) and upregulating SIRT3 expression levels (1.30 ± 0.05 AU vs. 0.44 ± 0.02 0mM; $P < 0.001$) in LoVo cells (Fig. 3K–O). Conversely, Egt treatment decreased SIRT3 protein expression (0.58 ± 0.03 AU vs. 0.95 ± 0.02 in 0mM, $P < 0.01$) in CCD 841 CoN cells (Fig. S4A). Interestingly, other sirtuins, such as SIRT1 and SIRT6, were modulated by Egt treatment
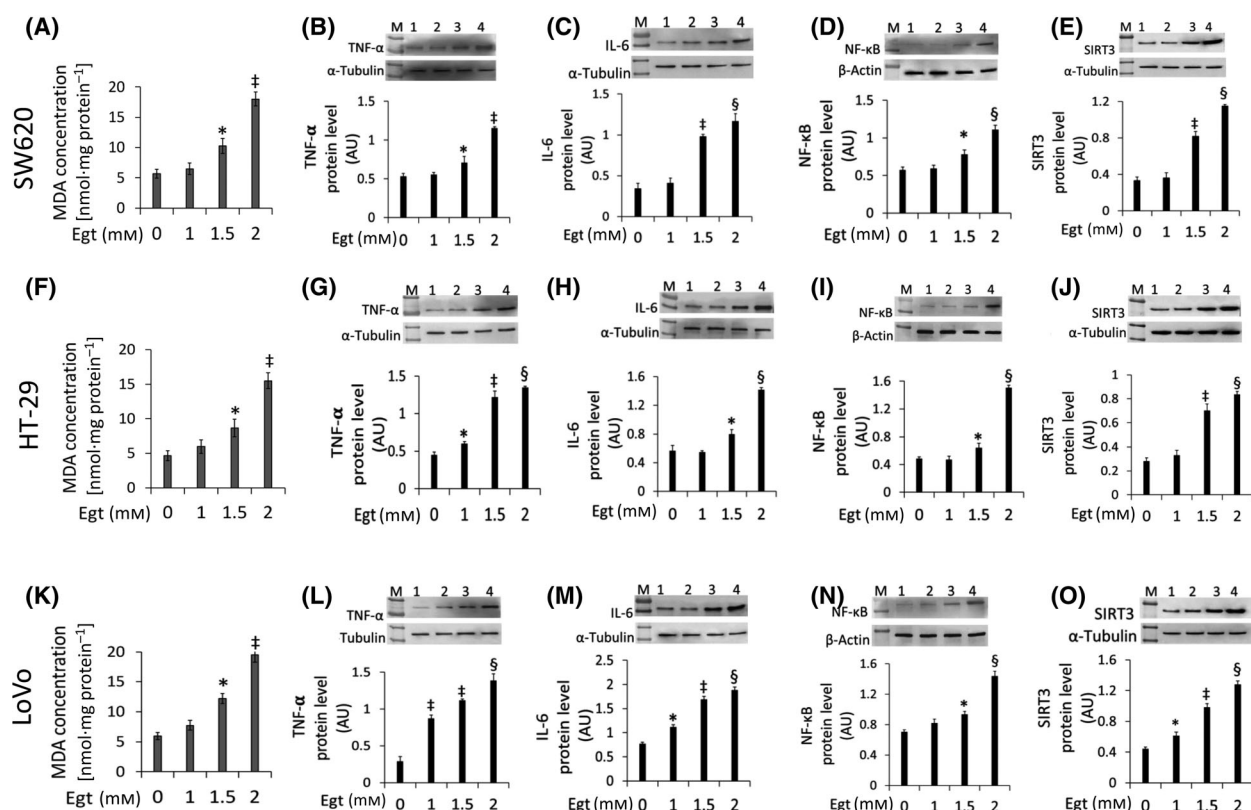
Fig. 3. Egt mediated inflammation, SIRT3 increase and lipid peroxidation in CRC cells. MDA cellular content and representative cropped blots with relative immunoblotting analysis of TNF-α, IL-6, NF-κB and SIRT3 in (A–E) SW620, (F–J) HT-29 and (K–O) LoVo cells. CRC cells were treated with 1, 1.5 and 2 mM Egt for 72 h. Control cells (0 mM) were grown in medium containing the higher corresponding volume of HBSS-10 mM Hepes. Lane 1 = 0 mM; lane 2 = 1 mM; lane 3 = 1.5 mM; lane 4 = 2 mM; M = weight markers (G266, Applied Biological Materials Inc.). Protein expression was calculated, after normalization with α-tubulin or β-actin as internal control, with IMAGEJ software, and results expressed as arbitrary units (AU). Data are shown as mean ± SD of $n = 3$ independent experiments. *$P < 0.05$ vs. 0 mM; ‡$P < 0.01$ vs. 0 mM; §$P < 0.001$ vs. 0 mM.

in CRC cells (Fig. S4). Egt treatment downregulated SIRT1 levels and upregulated SIRT6 protein expression in all CRC lines (Fig. S4B–G). The higher effects were observed in SW620 cells showing a negative modulation of SIRT1 (1.10 ± 0.04 AU vs. 1.68 ± 0.04 in 0mM) ($P < 0.01$) and a positive modulation of SIRT6 (2.12 ± 0.03 AU vs. 1.43 ± 0.02 in 0mM with) ($P < 0.001$).

Egt induced S phase accumulation in HT-29 and G2/M arrest in SW620 and LoVo cells

Cell cycle analysis showed that 72 h of treatment with 2mM Egt increased the G2/M population in SW620 cells ($43.03 \pm 3.26\%$ vs. $13.8 \pm 3.17\%$ cell population in 0mM, $P < 0.001$) and cyclin B protein degradation (0.74 ± 0.01 AU vs. 1.28 ± 0.04 in 0mM, $P < 0.001$) (Fig. 4A–C). Similar effects were obtained in LoVo cells, showing cell accumulation in G2/M phase ($31.16 \pm 3.71\%$ vs. $12.36 \pm 2.86\%$ of cell population in 0mM, $P < 0.001$) and cyclin B downregulation

(0.22 ± 0.03 AU vs. 1.39 ± 0.03 in 0mM, $P < 0.001$) (Fig. 4G–I). In HT-29 cells, Egt treatment induced S phase arrest ($57.33 \pm 7.5\%$ vs. $21.16 \pm 0.92\%$ of cell population in 0mM, $P < 0.001$) and upregulation of cyclin D protein expression (1.31 ± 0.07 AU vs. 0.30 ± 0.06 in 0mM, $P < 0.001$) (Fig. 4D–F). Less pronounced Egt effects on CRC cell cycle modulation were detected after 24 h and 48 h treatments (Fig. S5).

Egt differentially induced necrosis and apoptosis in CRC cells

Cell death mechanism following Egt treatment was assessed using the flow cytometry-based annexin V/PI method and by evaluation of acetylated p53 and procaspases-9, −3 and −8 protein expression levels. The annexin V/PI staining defined a strong necrosis rate in SW620 cells when treated with 2mM Egt for 72 h ($24.91 \pm 2.2\%$ vs. $4.51 \pm 1.1\%$ of cell population in 0mM, $P < 0.001$) (Fig. 5A,B). Immunoblotting analysis showed upregulation of procaspase-9 and
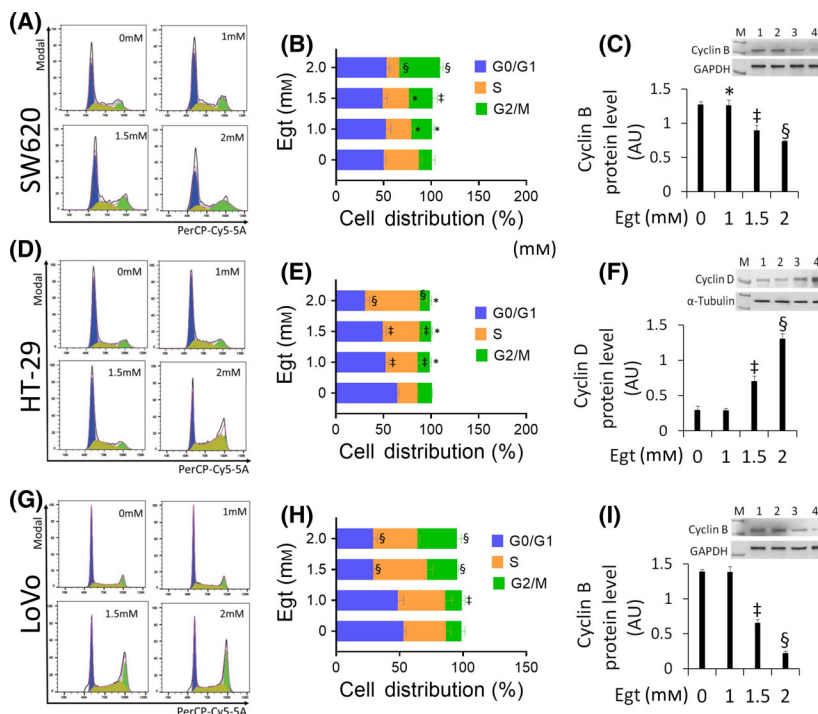
Fig. 4. Egt modulated CRC cell cycle. Representative cell cycle analysis and cropped blots of western blotting examination of cyclin B or cyclin D in (A–C) SW620, (D–F) HT-29 and (G–I) LoVo cells. CRC cells were treated with 1, 1.5 and 2 mM Egt for 72 h. Control cells (0 mM) were grown in medium containing the higher corresponding volume of HBSS-10 mM Hepes. Cell distribution was assessed by flow cytometry collecting PI fluorescence as FL3-A (linear scale). For each sample, at least 20 000 events were collected and analysis performed by using MODFIT software (Verity Software House, Becton Dickinson, Topsham, ME, USA). Lane 1 = 0 mM; lane 2 = 1 mM; lane 3 = 1.5 mM; lane 4 = 2 mM; M = weight markers (G266, Applied Biological Materials Inc.). Protein expression was calculated, after normalization with α-tubulin or GAPDH as internal control, with IMAGEJ software, and results expressed as arbitrary units (AU). Data are shown as mean $\pm$ SD of $n = 4$ independent experiments. *$P < 0.05$ vs. 0 mM; ‡$P < 0.01$ vs. 0 mM; §$P < 0.001$ vs. 0 mM.
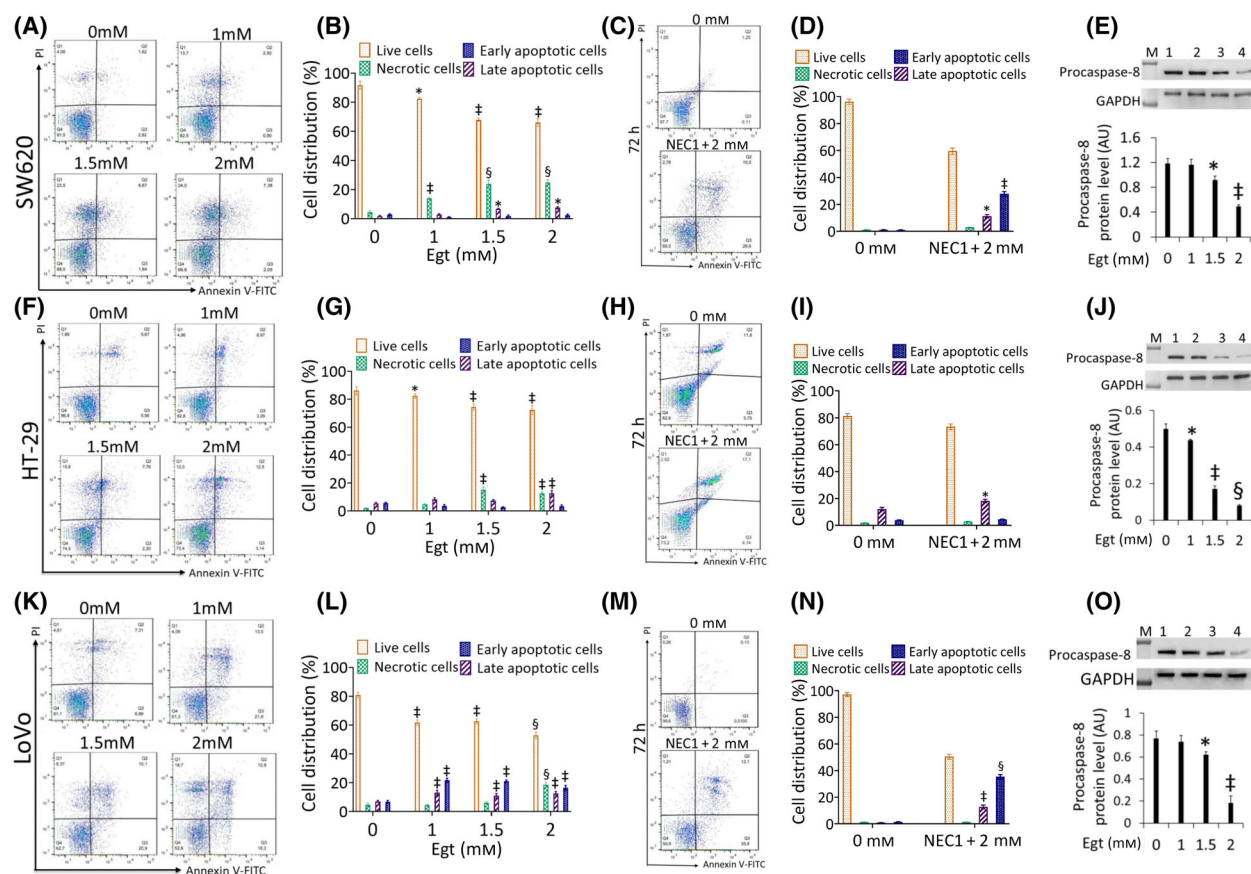
Fig. 5. Egt induced cell death in CRC cells. Representative dot plots and analyses of annexin V-FITC and propidium iodide (PI)-staining and cropped blots with relative immunoblotting analysis of procaspase-8 in (A–E) SW620, (F–J) HT-29 and (K–O) LoVo cells. CRC cells were treated with 1, 1.5 and 2 mm Egt or pretreated 1 h with NEC1 (50 μm) before Egt (2 mm) incubation for 72 h. Control cells (0 mm) were grown in medium containing the higher corresponding volume of HBSS-10 mm Hepes. Cell viability/death was assessed by flow cytometry acquiring at least 20 000 events. Lower left quadrant: viable cells; upper left quadrant: necrotic cells; lower right quadrant: early apoptotic cells; upper right quadrant: late apoptotic cells. Lane 1 = 0 mm; lane 2 = 1 mm; lane 3 = 1.5 mm; lane 4 = 2 mm; M = weight markers (G266, Applied Biological Materials Inc.). Protein expression was calculated, after normalization with GAPDH as internal control, with IMAGEJ software and results expressed as arbitrary units (AU). Data are expressed as mean ± SD of $n = 3$ experiments. $*P < 0.05$ vs. 0 mm; $‡P < 0.01$ vs. 0 mm; $§P < 0.001$ vs. 0 mm.

procaspase-3 ($P < 0.001$) (Fig. S6D,E) and downregulation of procaspase-8 ($P < 0.01$) (Fig. 5E). In HT-29 cell line, a rise in necrotic cells ($12.8 \pm 1.1\%$ vs. $1.98 \pm 0.3\%$ of cell population in 0mM, $P < 0.01$) (Fig. 5F,G), increase in procaspase-9 and procaspase-3 ($P < 0.001$) (Fig. S6J,K) and degradation of procaspase-8 protein level ($P < 0.001$) (Fig. 5J) were observed. Egt treatment contributed to necrotic cell death ($18.6 \pm 2.2\%$ vs. $4.7 \pm 1.6\%$ of cell population in 0mM, $P < 0.001$) (Fig. 5K,L), procaspase-9, procaspase-3 and acetylated p53 increase in protein expression ($P < 0.001$) (Fig. S6) and downregulation of procaspase-8 levels (Fig. 5O) also in LoVo cells. Less significant effects on apoptosis were detected in CRC cells when incubated with Egt for 24 h and 48 h (Fig. S6A–C, G–I and M–O). Noteworthy, the Egt

capability to trigger necrotic cell death in CRC cells was attenuated after pretreatment with necrostatin-1 (NEC1), a necroptosis inhibitor (Fig. 5C–D, H–I and M–N). Indeed, NEC1 shifted CRC cell death through apoptosis (late and early), thus lowering the per cent of necrotic population. These results suggested that the necrotic death observed in the presence of Egt was necroptosis, encouraging further investigation on the underlying signalling pathway.

Egt activated RIP1/RIP3/MLKL necroptosis signalling pathway

Western blot showed the Egt efficacy of positively modulating the expression levels of necroptotic key enzymes, RIP1, RIP3 and MLKL ($P < 0.001$) (Fig. 6).
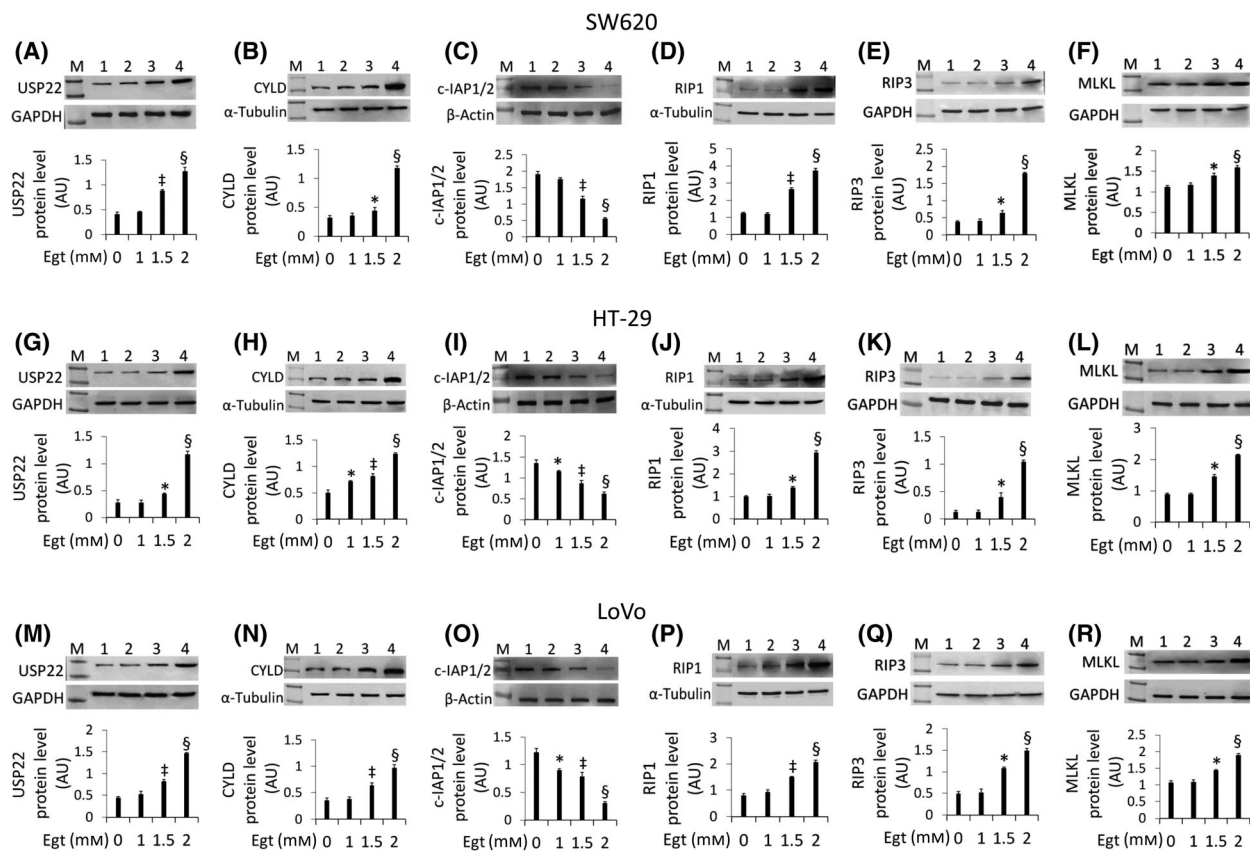
Fig. 6. Egt regulated necroptotic pathway in CRC cells. Representative cropped blots with relative immunoblotting analysis of USP22, CYLD, c-IAP1/2, RIP1, RIP3 and MLKL in (A–F) SW620, (G–L) HT-29 and (M–R) LoVo cells. CRC cells were treated with 1, 1.5 and 2 mM Egt for 72 h. Control cells (0 mM) were grown in medium containing the higher corresponding volume of HBSS-10 mM Hepes. Lane 1 = 0 mM; lane 2 = 1 mM; lane 3 = 1.5 mM; lane 4 = 2 mM; M = weight markers (G266, Applied Biological Materials Inc.). Protein expression was calculated, after normalization with α-tubulin, β-actin or GAPDH as internal control, with IMAGEJ software and results expressed as arbitrary units (AU). Data are expressed as mean ± SD of $n = 3$ experiments. *$P < 0.05$ vs. 0 mM; ‡$P < 0.01$ vs. 0 mM; §$P < 0.001$ vs. 0 mM.

These Egt effects on necroptosis markers were also accompanied by upregulation of the tumour suppressor ubiquitin-specific peptidase 22 (USP22) ($P < 0.001$) and cylindromatosis deubiquitinase (CYLD) ($P < 0.001$) protein levels, along with a strong degradation ($P < 0.001$) of cellular inhibitor of apoptosis protein 1 and 2 (c-IAP1/2) (Fig. 6).

## Egt induced SIRT3/MLKL protein interaction

We next investigated the possible SIRT3/MLKL interaction in preventing MLKL oligomerization and ability in forming pores which finally lead to disruption of plasma membrane integrity. SDS-denatured cell lysates were used to study MLKL/SIRT3 interaction by immunoprecipitation with MLKL antibody, followed by immunoblotting for SIRT3. Equal anti-MLKL immunoprecipitation was also monitored by re-

probing the membrane with anti-MLKL antibody. Results revealed an enhanced interaction between MLKL/SIRT3 in response to 1.5 mM Egt in CRC cell lines ($P < 0.01$). In addition, interplay between endogenous MLKL and SIRT3 proteins was markedly increased after treatment with 2mM Egt incubation ($P < 0.001$), accompanied with evident reduction in SIRT3 expression levels (Fig. 7), thus providing the interaction between these two proteins in a dose-dependent manner (Fig. 7).

Necroptosis and ROS accumulation induced by Egt occurred *via* SIRT3

To further confirm SIRT3 involvement in necroptosis pathway, transient SIRT3 gene silencing was performed before 2 mM Egt treatment (Fig. 8). Silencing of SIRT3 determined a consistent decrease in RIP1
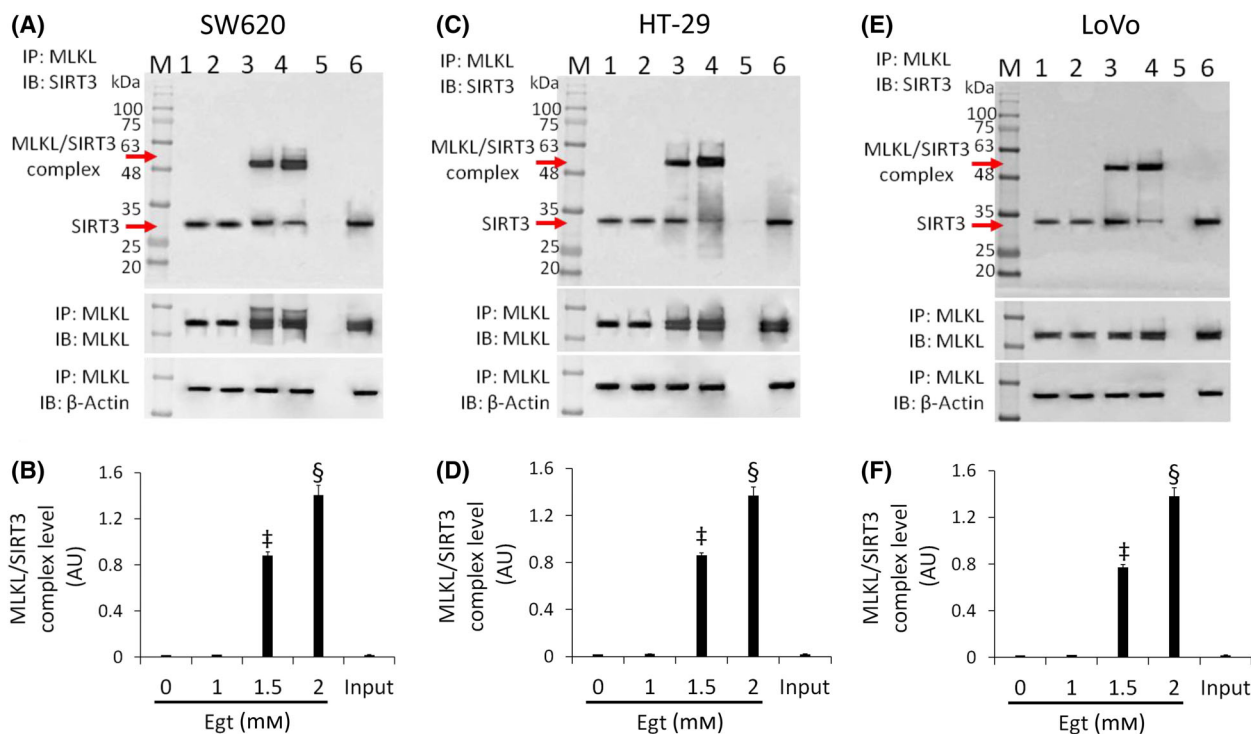
Fig. 7. Egt induced MLKL/SIRT3 interaction in CRC cells. The interaction between MLKL and SIRT3 was detected by IP analysis in (A-B) SW620, (C-D) HT-29 and (E-F) LoVo cells. CRC cells were treated with Egt for 72 h while control (0 mM) was grown in medium containing the higher corresponding volume of HBSS-10 mM Hepes. SDS-denatured cell lysates (200 µg) were used for MLKL/SIRT3 interaction by immunoprecipitation with MLKL antibody followed by immunoblotting for SIRT3. Equal anti-MLKL immunoprecipitation was monitored by re-probing the membrane with anti-MLKL antibody. Equal protein input for immunoprecipitation was also reported. Lane 1 = 0 mM; lane 2 = 1 mM; lane 3 = 1.5 mM; lane 4 = 2 mM; lane 5 = protein A/G sepharose; lane 6 = input (whole cell lysate); M = weight markers (G266, Applied Biological Materials Inc.) Protein expression was calculated, after normalization with β-actin as internal control, with IMAGEJ software and results expressed as arbitrary units (AU). Data are expressed as mean ± SD of n = 3 experiments. $^{\ddagger}P < 0.01$ vs. 0 mM; $^{\S}P < 0.001$ vs. 0 mM.

and MLKL expression levels and attenuated their accumulation induced by Egt, suggesting that necroptosis occurs *via* SIRT3 upregulation (Fig. 8). Analysis of annexin V/PI staining revealed that SIRT3 silencing determined apoptotic death accumulation in SW620, HT-29 and LoVo cells (19.53 ± 2.7 vs. 4.71 ± 1.3%; 22.58 ± 3.45 vs. 6.82 ± 1.15%; 34.0 ± 5.12 vs. 7.29 ± 1.31% of Ctr, $P < 0.001$), thus overriding the Egt-induced necroptosis and suggesting that this mechanism is SIRT3 dependent (Fig. 8). Finally, SIRT3 silencing counteracted the increase in ROS induced by Egt treatment at mitochondrial and intracellular levels, suggesting an upstream role of this sirtuin in the oxidative stress triggered by Egt (Fig. S7).

Discussion

In this study we provided the first evidence on the *in vitro* anti-cancer activity of Egt in CRC cells. Egt treatment displayed cytotoxic and apoptotic effects in CRC cells after 72 h of treatment in a dose-dependent

manner. LoVo, HT-29 and SW620 cells were chosen as having different characteristics, with LoVo and SW620 known to be highly metastatic when compared with HT-29, whereas HT-29 cells are more adhesive than other colon cancer cells. The same dosage and exposure time as that used on CRC cell lines showed no adverse effects on normal CCD 841 CoN cells, suggesting that Egt was not cytotoxic in non-cancerous cells. Our results showed that Egt (2mM) for 72 h provoked a ROS accumulation at intracellular, extracellular and mitochondrial levels, impaired the MMP and affected the CRC tumour microenvironment by increasing TNF-α, IL-6 and NF-κB protein expression levels. Although the evidence for one-electron oxidant formation in extracellular and intracellular settings has to be obtained by determining dimeric product formation using HPLC and LC-MS techniques [33], the global profile of oxidation products here performed, to fully assess the extracellular, intracellular and mitochondrial oxidant formation, suggested the pro-oxidant role of Egt in CRC cells. The
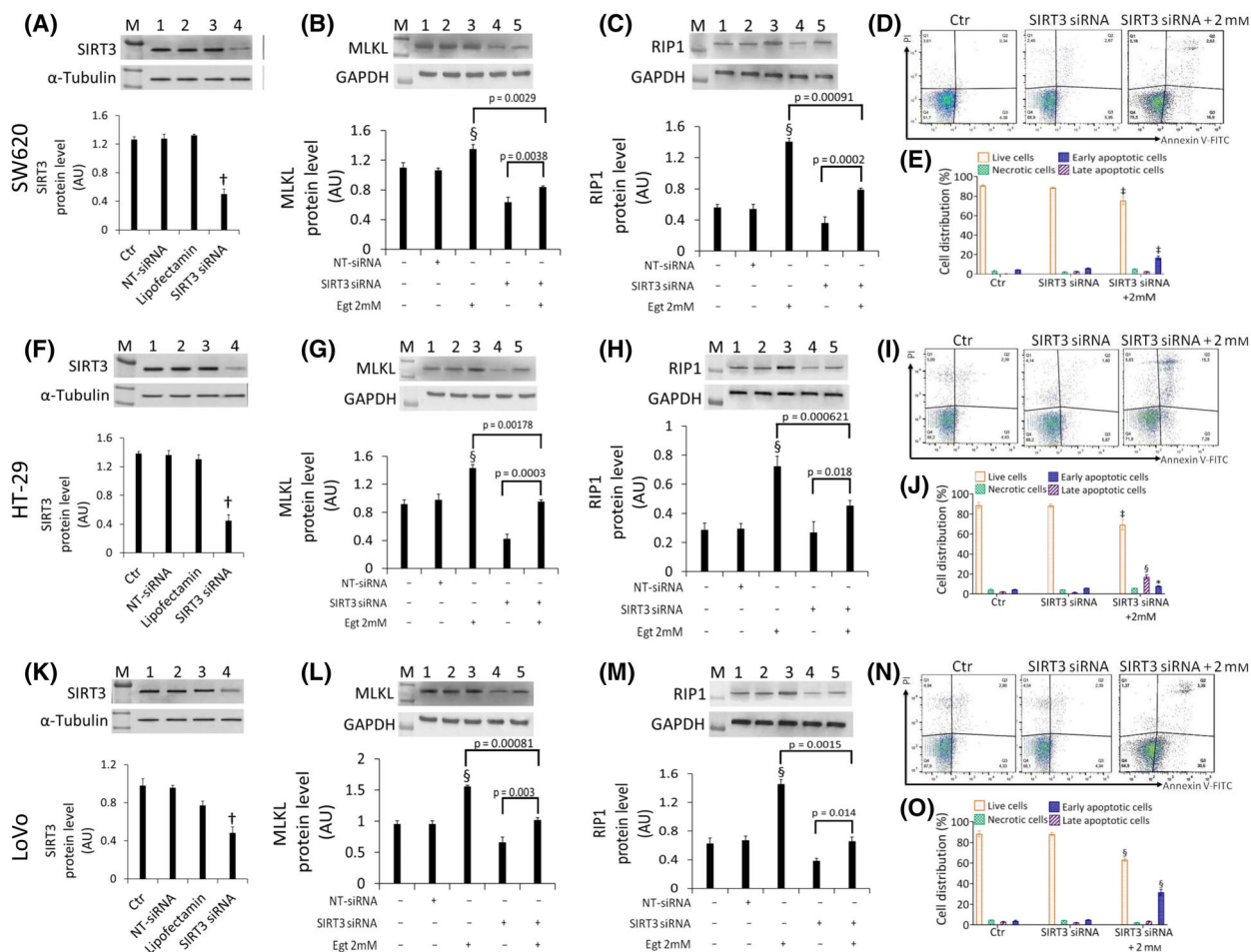
Fig. 8. Egt triggered necroptosis in CRC cells *via* SIRT3. CRC cells were transfected with scramble siRNA (NT-siRNA), transfection reagent (lipofectamin) and SIRT3 siRNA, and protein expression levels of SIRT3 in (A) SW620, (F) HT-29 and (K) LoVo were assessed by immunoblotting analysis. Lane 1 = Ctr; lane 2 = NT-siRNA; lane 3 = lipofectamin; Lane 4 = SIRT3 siRNA; M = weight markers (G266, Applied Biological Materials Inc.). $^{†}P < 0.01$ vs. Ctr. After SIRT3 silencing, CRC cells were treated with 2 mM Egt for 72 h. MLKL and RIP1 expression levels were determined by immunoblotting analysis while representative dot plots and analyses of annexin V-FITC and PI-staining were assessed by flow cytometry in (B–E) SW620, (G–J) HT-29 and (L–O) LoVo cells. Cell viability/death was assessed by flow cytometry acquiring at least 20 000 events. Lower left quadrant: viable cells; upper left quadrant: necrotic cells; lower right quadrant: early apoptotic cells; upper right quadrant: late apoptotic cells. Lane 1 = Ctr; lane 2 = NT-siRNA; lane 3 = 2 mM Egt for 72 h; lane 4 = SIRT3 siRNA; lane 5 = SIRT3 siRNA + 2 mM Egt for 72 h; M = weight markers (G266, Applied Biological Materials Inc.). Protein expression was calculated after normalization with GAPDH or α-tubulin as internal control, with IMAGEJ software, and results expressed as arbitrary units (AU). Data are expressed as mean ± SD of $n = 3$ experiments. $*P < 0.05$ vs. 0 mM; $^{‡}P < 0.01$ vs. 0 mM; $^{§}P < 0.001$ vs. 0 mM.

Egt-induced pro-oxidant and pro-inflammatory effects were accompanied by an increase in SIRT3 protein content (Fig. 9).

In CRC, SIRT3 represents a therapeutic target with oncogenic and tumour-suppressive role. The SIRT3 tumour-suppressive role in CRC was demonstrated both *in vitro* [24] and *in vivo* using SIRT3 knockout mice, showing increased intestinal polyp numbers and severity of colonic proliferation with abolished SIRT3 compared to wild-type mice, together with decreased caspase-3 activation, thus confirming a tumour-suppressive role of SIRT3 in gut inflammation and CRC development [34].

Inflammation associated with tumours is a key feature in CRC since inflammatory mediators, proper of the tumour microenvironment, are in crosstalk between immunity and cancer cells. TNF-α plays an important role in CRC progression and, in combination with IL-32γ, notably inhibited cell growth of HCT116 and SW620 cells and tumour growth in xenograft-bearing nude mice [35]. Increased TNF-α triggered expression of p38 MAPK, as well as that of
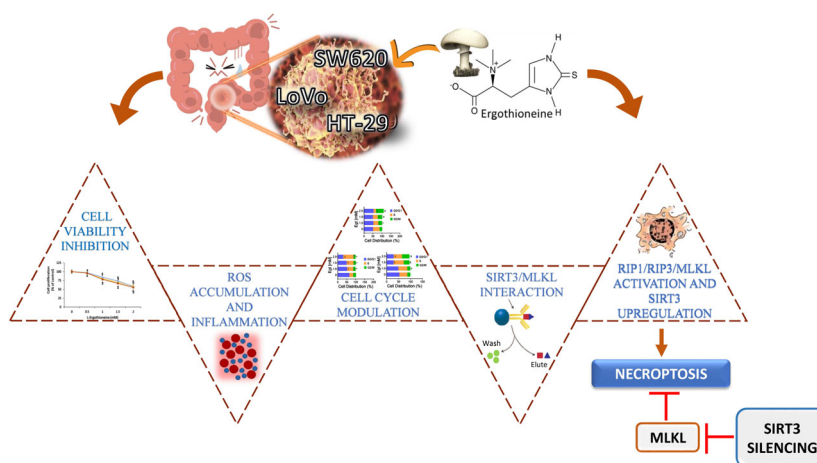
Fig. 9. Proposed schematic representation of Egt-mediated effects in CRC cells. Necroptosis induced by Egt was reverted by SIRT3 silencing, suggesting a fundamental role of the mitochondrial sirtuin in the anti-proliferative and cytotoxic outcome.

Bax, cleaved caspase-3 and −9, along with decrease in anti-apoptotic proteins such as Bcl-2 and c-IAP in CRC cell lines [35]. In HCT116, the TNF-α-induced DNA damage by activation of JNK signalling pathway leads to pre-apoptotic events [36]]. As inflammatory player, NF-κB regulates the expression of genes involved in various functions including cell survival and immune response and is often constitutively activated in CRC [37]. The persistent activation of NF-κB revealed to upregulate pro-apoptotic functions shifting the balance towards death in intestinal cells [38]. More recently, evidence revealed that NF-κB alone plays a pro-apoptotic role concomitant with aberrant Wnt signalling in mouse intestinal epithelial cells [39]. Our data provided new knowledge on inflammation-induced cell death in CRC and unveiled the specific cell death mechanism occurring under Egt treatment. Results showed that the anti-tumour effects of Egt occurred *via* a necroptosis mechanism linked to SIRT3/MLKL pathway. IP assay unveiled that the interaction between MLKL and SIRT3 was augmented during the Egt treatment. Intriguingly, SIRT3 silencing by small interfering RNA opposed the effect of Egt on MLKL and RIP3 protein expression levels and necroptosis activation, suggesting that this mechanism is, at least in part, directly mediated by SIRT3 (Fig. 9). In this study, Egt-induced necroptosis and cytotoxicity was mediated by ROS accumulation, as well as the activation of RIP1-RIP3-MLKL. The antioxidant NAC blocked the cell viability inhibition, and NEC-1, a specific inhibitor of RIP1, suppressed the number of PI-positive CRC cells. Along with the activation of RIP1/RIP3/MLKL signalling, Egt down-regulated cIAP1/2 protein level, the anti-apoptotic proteins that exert their function by binding to and inhibiting effector caspase-9 and −3/-7 [40], and upregulated USP22, a member of the so-called 11-gene

'death-from-cancer' expression signature, associated with distant metastasis, worse prognosis and poor patient survival in CRC [41]. The Egt was also effective in inducing the tumour suppressor CYLD protein expression whose downregulation has been associated with the development of multiple carcinoma and CRC [42]. An important aspect of the contribution of CYLD to tissue homeostasis is its ability to modulate programmed cell death by apoptosis and necroptosis. Indeed, CYLD has been identified as an important mediator of necroptosis, which relies on its ability to deubiquitinate RIP1 and to facilitate its phosphorylation along with the phosphorylation of RIP3 [43]. High levels of ROS mediate necroptotic cell death by increasing the RIP1 and RIP3 levels and their reciprocal binding, promoting necrosome formation [44,45]. As a consequence, RIP3, linked to the plasma membrane, promotes the phosphorylation of MLKL, which induces the oligomerization of p-MLKL to induce plasma membrane rupture and necroptosis [46]. In CRC, low RIP3 expression levels have been found associated with poor clinical outcome and survival of CRC patients [47], although different studies suggested that loss of RIPK3 does not affect CRC development [48]. In CRC cells, overexpression of RIP3 in human RKO colon cancer cells was related to induction of apoptosis, inhibition of proliferation, attenuation of migration and invasion [47]. Moreover, RIP3 mediates the MLKL activation which, in turn, resulted upregulated by Egt treatment. MLKL activation occurs by phosphorylation of threonine 357 and serine 358 on the activation loop, which mitigates the auto-inhibitory monomer state of MLKL and promotes its oligomerization and translocation to plasma membranes, where it forms pores and disrupts plasma membrane integrity, leading to necroptosis [28,49,50]. Low MLKL expression has been shown to be

associated with poor prognosis of CRC, and administration of MLKL mRNA inhibited tumour growth [51]. The dimerization of the kinase-like domain of MLKL represents the critical step to induce oligomerization and activation of full-length protein, but the transition from monomer to oligomer of the coiled-coil region controlled by kinase-like domain is still uncovered [48]. The critical role of MLKL in cancer, more than as a necroptosis regulator, has been investigated by Martens S et al [52]. To date, no epigenetic silencing mechanisms have been reported for MLKL and no acetylated sites have been described. Results of this study lead us to speculate a physical interaction between SIRT3 and MLKL that could facilitate MLKL oligomerization. Indeed, in CRC cells, Egt was effective in determining MLKL/SIRT3 protein interaction which was blocked by SIRT3 transient gene silencing, thus inhibiting the necroptosis.

The peculiar antioxidant activities of Egt in scavenging hydroxyls and other free radicals are distinguished by its ability to be irreversibly oxidized by relevant oxidants occurring in cells, making this betaine a major antioxidant when the body is placed under higher oxidative stress [53,54]. Indeed, Egt accumulates in various organs and tissues in mice [11] and humans [54], especially in the liver, as well as in kidney, heart, spleen, intestines, eye and brain tissues. A pharmacokinetic study using encapsulated Egt (5 and 25 mg·day^{-1}) on healthy humans reported that Egt is rapidly absorbed and largely retained by the body, especially in plasma, while only minimal increases (< 4%) in urinary excretion was observed [54]. A population-based prospective cohort study reported that, among the 112 healthy dietary measured metabolites, Egt plasma levels were strongly and independently associated with the health-conscious food pattern, correlated with protection from cardiovascular disease and type 2 diabetes and a lower risk of future coronary artery disease and cardiovascular and all-cause mortality [7]. Moreover, an inverse correlation of blood and plasma Egt levels has been found with age [4], reporting a mean plasma Egt values of 442.8 ± 30.9 for subjects below the age of 65, 413.8 ± 30.4 in 65–70 age group, 393.4 ± 31.2 in age 71–75 and 275.5 ± 20.7 nM in above 75 age group, thus demonstrating a significant decline with increasing age [4]. The increase in oxidative damage occurring with ageing and age-related disease, including CRC, could in part be explained by the declining levels of Egt. Although, the concentration of Egt (2 mM) used in the present *in vitro* study was higher than the concentration resulting from dietary intake, a single-centre, randomised, double-blind, placebo-controlled,

pilot intervention trial (ISRCTN, ISRCTN25890011 Registered February 10th, 2021) has been recently designed to supplement participants with metabolic syndrome with 5 or 30 mg·day^{-1} Egt for 12 weeks [55]. Egt represents a rich free source of reducing equivalents, with antioxidant and metal chelating properties utilized continuously under basal cellular conditions, protecting endothelial cells during intensive ROS accumulation [9]. Copper and iron, two essential metals accumulated in cancer cells, are involved in the rapid proliferation of cancer cells promoting angiogenesis and metastasis [56,57]. In this scenario, we speculated that Egt could selectively affect CRC cells through redox cycling, generation of ROS and metal deprivation.

The genetic features of cell lines used in this study (HT-29 that mimics a primary colon adenocarcinoma, and a metastatic site (Dukes' type B and D), SW620 and LoVo) could explain the selective responsiveness to Egt. Indeed, differences in tumour microenvironment might translate into distinct responsiveness to cell death. Persistent oxidative stress is a common feature of CRC cells which is known to be exacerbated by some natural antioxidant [58,59]. It is undoubtedly intriguing how the antioxidant Egt induces ROS, which itself seem to fail to quench completely, causing CRC cell death. At present, the Egt mechanism of cytotoxicity remains unsolved, as well as its specificity for CRC. One possible explanation could be that Egt, acting as iron-chelating agent, could interfere with the Fenton reaction, thus leading to enhanced formation of ROS, especially highly reactive hydroxyl radical. Therefore, Egt could exhibit a pro-oxidative effect in CRC cells by driving the Fenton reaction forward and promoting the reducing Fe^{3+} reaction, thus producing more free radicals, as for ascorbic acid and the flavonoid (-)-epigallocatechin gallate [60,61]. Altogether, the present *in vitro* study represents the first evidence of the role of dietary Egt in inducing necroptosis in CRC cells, HT-29, LoVo and SW620, supporting its potential in the prevention of CRC. Silencing experiments suggested that SIRT3 could mediate Egt-induced cell death.

Finally, despite the killing of Egt mechanism is not fully known, the pro-oxidant and anti-cancer action of Egt involves SIRT3 protein upregulation. Although SIRT3 was reported to be protective against cell death, it has been recently shown that the overexpression of this sirtuin resulted in metabolic reprogramming and triggering cell death in CRC and necroptosis activation in small-cell lung cancer by controlling the ubiquitination of mutant p53 [24,62]. However, further studies on CRC cells overexpressing SIRT3 are necessary to

definitely clarify whether SIRT3 is a critical mediator of Egt-induced necroptosis. Additional studies will be also crucial in deepening the knowledge on the molecular mechanism and in providing *in vivo* evidence on the anti-cancer properties of Egt in CRC.

Acknowledgements

Author contributions

Conceptualization, ND and MLB methodology, ND and EM validation, ND, EM, LM, formal analysis, AB, D Castaldo, and D Cautela, writing–original draft preparation, ND and MLB writing-review and editing, ND and MLB supervision, MLB All authors have read and agreed to the published version of the manuscript.

Data accessibility

The data supporting the findings of this article are available from the corresponding author upon reasonable request.

References

1 Halliwell B, Cheah IK, Tang RMY. Ergothioneine – a diet-derived antioxidant with therapeutic potential. *FEBS Lett*. 2018;**592**:3357–66.

2 Paul BD. Ergothioneine: a stress vitamin with antiaging, vascular, and neuroprotective roles? *Antioxid Redox Signal*. 2021. doi:10.1089/ars.2021.0043. Online ahead of print.

3 Sakrak O, Kerem M, Bedirli A, Pasaoglu H, Akyurek N, Ofluoglu E, et al. Ergothioneine modulates proinflammatory cytokines and heat shock protein 70 in mesenteric ischemia and reperfusion injury. *J Surg Res*. 2008;**144**:36–42.

4 Cheah I, Feng L, Tang RMY, Lim KHM, Halliwell B. Ergothioneine levels in an elderly population decrease with age and incidence of cognitive decline; a risk factor for neurodegeneration? *Biochem Biophys Res Commun*. 2016;**478**:162–7.

5 Servillo L, D'Onofrio N, Balestrieri ML. Ergothioneine antioxidant function: from chemistry to cardiovascular therapeutic potential. *J Cardiovasc Pharmacol*. 2017;**69**:183–91.

6 Shinozaki Y, Furuichi K, Toyama T, Kitajima S, Hara A, Iwata Y, et al. Impairment of the carnitine/organic cation transporter 1-ergothioneine axis is mediated by intestinal transporter dysfunction in chronic kidney disease. *Kidney Int*. 2017;**92**:1356–69.

7 Smith E, Ottosson F, Hellstrand S, Ericson U, Orho-Melander M, Fernandez C, et al. Ergothioneine is associated with reduced mortality and decreased risk of cardiovascular disease. *Heart*. 2020;**106**:691–7.

8 Ba DM, Gao X, Al-Shaar L, Muscat J, Chinchilli VM, Ssentongo P, et al. Prospective study of dietary mushroom intake and risk of mortality: results from continuous National Health and Nutrition Examination Survey (NHANES) 2003–2014 and a meta-analysis. *Nutr J*. 2021;**20**:80.

9 D'Onofrio N, Servillo L, Giovane A, Casale R, Vitiello M, Marfella R, et al. Ergothioneine oxidation in the protection against high-glucose induced endothelial senescence: involvement of SIRT1 and SIRT6. *Free Radic Biol Med*. 2016;**96**:211–22.

10 Lamhonwah AM, Tein I. Novel localization of OCTN1, an organic cation/carnitine transporter, to mammalian mitochondria. *Biochem Biophys Res Commun*. 2006;**345**:1315–25.

11 Tang RMY, Cheah IK, Yew TSK, Halliwell B. Distribution and accumulation of dietary ergothioneine and its metabolites in mouse tissues. *Sci Rep*. 2018;**8**:1601.

12 Tschirka J, Kreisor M, Betz J, Grundemann D. Substrate selectivity check of the ergothioneine transporter. *Drug Metab Dispos*. 2018;**46**:779–85.

13 Okabe M, Szakács G, Reimers MA, Suzuki T, Hall MD, Abe T, et al. Profiling SLCO and SLC22 genes in the NCI-60 cancer cell lines to identify drug uptake transporters. *Mol Cancer Ther*. 2008;**7**:3081–91.

14 Juraszek B, Nalecz KA. SLC22A5 (OCTN2) carnitine transporter-indispensable for cell metabolism, a Jekyll and Hyde of human cancer. *Molecules*. 2019;**25**:14.

15 Martini M, Ferrara AM, Giachelia M, Panieri E, Siminovitch K, Galeotti T, et al. Association of the OCTN1/1672T variant with increased risk for colorectal cancer in young individuals and ulcerative colitis patients. *Inflamm Bowel Dis*. 2012;**18**:439–48.

16 Zou D, Lou J, Ke J, Mei S, Li J, Gong Y, et al. Integrative expression quantitative trait locus-based analysis of colorectal cancer identified a functional polymorphism regulating SLC22A5 expression. *Eur J Cancer*. 2018;**93**:1–9.

17 NavaneethaKrishnan S, Rosales JL, Lee KY. ROS-mediated cancer cell killing through dietary phytochemicals. *Oxid Med Cell Longev*. 2019;**2019**:1–16.

18 D'Onofrio N, Cacciola NA, Martino E, Borrelli F, Fiorino F, Lombardi A, et al. ROS-mediated apoptotic cell death of human colon cancer LoVo cells by milk δ-valerobetaine. *Sci Rep*. 2020;**10**:8978.

19 D'Onofrio N, Martino E, Mele L, Colloca A, Maione M, Cautela D, et al. Colorectal cancer apoptosis induced by dietary δ-valerobetaine involves PINK1/Parkin dependent-mitophagy and SIRT3. *Int J Mol Sci*. 2021;**22**:8117.

20 Sung H, Ferlay J, Siegel RL, Laversanne M, Soerjomataram I, Jemal A, et al. Global cancer statistics 2020: GLOBOCAN estimates of incidence and mortality worldwide for 36 cancers in 185 countries. *CA Cancer J Clin*. 2021;**71**:209–49.

21 Garmpis N, Damaskos C, Garmpi A, Nonni A, Georgakopoulou VE, Antoniou E, et al. Histone deacetylases and their inhibitors in colorectal cancer therapy: current evidence and future considerations. *Curr Med Chem*. 2021. doi:10.2174/0929867328666210915105929. Online ahead of print.

22 Hirschey MD, Shimazu T, Goetzman E, Jing E, Schwer B, Lombard DB, et al. SIRT3 regulates mitochondrial fatty-acid oxidation by reversible enzyme deacetylation. *Nature*. 2010;**464**:121–5.

23 Li M, Chiang YL, Lyssiotis CA, Teater MR, Hong JY, Shen H, et al. Non-oncogene addiction to SIRT3 plays a critical role in lymphomagenesis. *Cancer Cell*. 2019;**35**:916–31.

24 D'Onofrio N, Martino E, Balestrieri A, Mele L, Neglia G, Balestrieri ML, et al. SIRT3 and metabolic reprogramming mediate the antiproliferative effects of whey in human colon cancer cells. *Cancers*. 2021;**13**:5196.

25 Holler N, Zaru R, Micheau O, Thome M, Attinger A, Valitutti S, et al. Fas triggers an alternative, caspase-8-independent cell death pathway using the kinase RIP as effector molecule. *Nat Immunol*. 2000;**1**:489–95.

26 Zhang DW, Shao J, Lin J, Zhang N, Lu BJ, Lin SC, et al. RIP3, an energy metabolism regulator that switches TNF-induced cell death from apoptosis to necrosis. *Science*. 2009;**325**:332–6.

27 Vandenabeele P, Galluzzi L, Vanden Berghe T, Kroemer G. Molecular mechanisms of necroptosis: an ordered cellular explosion. *Nat Rev Mol Cell Biol*. 2010;**11**:700–14.

28 Sun L, Wang H, Wang Z, He S, Chen S, Liao D, et al. Mixed lineage kinase domain-like protein mediates necrosis signaling downstream of RIP3 kinase. *Cell*. 2012;**148**:213–27.

29 Petrie EJ, Hildebrand JM, Murphy JM. Insane in the membrane: a structural perspective of MLKL function in necroptosis. *Immunol Cell Biol*. 2017;**95**:152–9.

30 Fulda S. Regulation of necroptosis signaling and cell death by reactive oxygen species. *Biol Chem*. 2016;**397**:657–60.

31 Zhao X, Quan J, Tan Y, Liu Y, Liao C, Li Z, et al. RIP3 mediates TCN-induced necroptosis through activating mitochondrial metabolism and ROS production in chemotherapy-resistant cancers. *Am J Cancer Res*. 2021;**11**:729–45.

32 Yan J, Wan P, Choksi S, Liu ZG. Necroptosis and tumor progression. *Trends Cancer*. 2022;**8**:21–27. Online ahead of print.

33 Kalyanaraman B. Pitfalls of Reactive Oxygen Species (ROS) measurements by fluorescent probes and mitochondrial superoxide determination using MitoSOX. In: Berliner LJ, Parinandi NL, editors. Measuring oxidants and oxidative stress in biological systems. Chapter 2. Cham: Springer; 2020:7–9.

34 Zhang Y, Wang XL, Zhou M, Kang C, Lang HD, Chen MT, et al. Crosstalk between gut microbiota and Sirtuin-3 in colonic inflammation and tumorigenesis. *Exp Mol Med*. 2018;**50**:1–11.

35 Park ES, Yoo JM, Yoo HS, Yoon DY, Yun YP, Hong J. IL-32gamma enhances TNF-alpha-induced cell death in colon cancer. *Mol Carcinog*. 2014;**53**:E23–35.

36 Alotaibi AG, Li JV, Gooderham NJ. Tumour necrosis factor-alpha (TNF-alpha) enhances dietary carcinogen-induced DNA damage in colorectal cancer epithelial cells through activation of JNK signaling pathway. *Toxicology*. 2021;**457**:152806.

37 Cardoso Alves L, Corazza N, Micheau O, Krebs P. The multifaceted role of TRAIL signaling in cancer and immunity. *FEBS J*. 2021;**288**:5530–54.

38 Guma M, Stepniak D, Shaked H, Spehlmann ME, Shenouda S, Cheroutre H, et al. Constitutive intestinal NF-κB does not trigger destructive inflammation unless accompanied by MAPK activation. *J Exp Med*. 2011;**208**:1889–900.

39 Mikuda N, Schmidt-Ullrich R, Kärgel E, Golusda L, Wolf J, Höpken UE, et al. Deficiency in Ikappa B alpha in the intestinal epithelium leads to spontaneous inflammation and mediates apoptosis in the gut. *J Pathol*. 2020;**251**:160–74.

40 Fulda S, Vucic D. Targeting IAP proteins for therapeutic intervention in cancer. *Nat Rev Drug Discov*. 2012;**11**:109–24.

41 Glinsky GV, Berezovska O, Glinskii AB. Microarray analysis identifies a death-from-cancer signature predicting therapy failure in patients with multiple types of cancer. *J Clin Invest*. 2005;**115**:1503–21.

42 Hellerbrand C, Bumes E, Bataille F, Dietmaier W, Massoumi R, Bosserhoff AK. Reduced expression of CYLD in human colon and hepatocellular carcinomas. *Carcinogenesis*. 2007;**28**:21–7.

43 Moquin DM, McQuade T, Chan FKM. CYLD deubiquitinates RIP1 in the TNFalpha-induced necrosome to facilitate kinase activation and programmed necrosis. *PLoS One*. 2013;**8**:e76841.

44 Belizário J, Vieira-Cordeiro L, Enns S. Necroptotic cell death signaling and execution pathway: lessons from knockout mice. *Mediators Inflamm*. 2015;**2015**:128076.

45 Lu B, Gong X, Wang ZQ, Ding Y, Wang C, Luo TF, et al. Shikonin induces glioma cell necroptosis in vitro by ROS overproduction and promoting RIP1/RIP3 necrosome formation. *Acta Pharmacol Sin*. 2017;**38**:1543–53.

46 Zhang Y, Chen X, Gueydan C, Han J. Plasma membrane changes during programmed cell deaths. *Cell Res*. 2018;**28**:9–21.

47 Feng X, Song Q, Yu A, Tang H, Peng Z, Wang X. Receptor-interacting protein kinase 3 is a predictor of survival and plays a tumor suppressive role in colorectal cancer. *Neoplasma*. 2015;**62**:592–601.

48 Alvarez-Diaz S, Preaudet A, Samson AL, Nguyen PM, Fung KY, Garnham AL, et al. Necroptosis is dispensable for the development of infammation-associated or sporadic colon cancer in mice. *Cell Death Differ*. 2021;**28**:1466–76.

49 Wang H, Sun L, Su L, Rizo J, Liu L, Wang LF, et al. Mixed lineage kinase domain-like protein MLKL causes necrotic membrane disruption upon phosphorylation by RIP3. *Mol Cell*. 2014;**54**:133–46.

50 Dondelinger Y, Declercq W, Montessuit S, Roelandt R, Goncalves A, Bruggeman I, et al. MLKL compromises plasma membrane integrity by binding to phosphatidylinositol phosphates. *Cell Rep*. 2014;**7**:971–81.

51 Li X, Guo J, Ding AP, Qi WW, Zhang PH, Lv J, et al. Association of mixed lineage kinase domain-like protein expression with prognosis in patients with colon cancer. *Technol Cancer Res Treat*. 2017;**16**:428–34.

52 Martens S, Bridelance J, Roelandt R, Vandenabeele P, Takahashi N. MLKL in cancer: more than a necroptosis regulator. *Cell Death Differ*. 2021;**28**:1757–72.

53 Servillo L, Castaldo D, Casale R, D'Onofrio N, Giovane A, Cautela D, et al. An uncommon redox behavior sheds light on the cellular antioxidant properties of ergothioneine. *Free Radic Biol Med*. 2015;**79**:228–2363.

54 Cheah IK, Tang RMY, Yew TS, Lim KC, Halliwell B. Administration of pure ergothioneine to healthy human subjects; Uptake, metabolism and effects on biomarkers of oxidative damage and inflammation. *Antioxid Redox Signal*. 2017;**26**:193–206.

55 Tian X, Cioccoloni G, Sier JH, Naseem KM, Thorne JL, Moore JB. Ergothioneine supplementation in people with metabolic syndrome (ErgMS): protocol for a randomised, double-blind, placebo-controlled pilot study. *Pilot Feasibility Study*. 2021;**7**:193.

56 Lovejoy DB, Jansson PJ, Brunk UT, Wong J, Ponka P, Richardson DR. Antitumor activity of metal-chelating compound Dp44mT is mediated by formation of a redox-active copper complex that accumulates in lysosomes. *Cancer Res*. 2011;**71**:5871–80.

57 Gupte A, Mumper RJ. Elevated copper and oxidative stress in cancer cells as a target for cancer treatment. *Cancer Treat Rev*. 2009;**35**:32–46.

58 Monteiro HP, Rodrigues EG, Amorim Reis AKC, Longo LS Jr, Ogata FT, Moretti AIS, et al. Nitric oxide and interactions with reactive oxygen species in the development of melanoma, breast, and colon cancer: a redox signaling perspective. *Nitric Oxide*. 2019;**89**:1–13.

59 Kundaktepe BP, Sozer V, Durmus S, Kocael PC, Kundaktepe FO, Papila C, et al. The evaluation of oxidative stress parameters in breast and colon cancer. *Medicine (Baltimore)*. 2021;**100**:e25104.

60 Szarka A, Kapuy O, Lőrincz T, Bánhegyi G. Vitamin C and cell death. *Antioxid Redox Signal*. 2021;**34**:831–44.

61 Slika H, Mansour H, Wehbe N, Nasser SA, Iratni R, Nasrallah G, et al. Therapeutic potential of flavonoids in cancer: ROS-mediated mechanisms. *Biomed Pharmacother*. 2022;**146**:112442.

62 Tang X, Li Y, Liu L, Guo R, Zhang P, Zhang Y, et al. Sirtuin 3 induces apoptosis and necroptosis by regulating mutant p53 expression in small-cell lung cancer. *Oncol Rep*. 2020;**43**:591–600.

Supporting information

Additional supporting information may be found online in the Supporting Information section at the end of the article.

Fig. S1. Egt effects on cell viability.

Fig. S2. Egt triggered oxidative stress in CRC lines but not in normal cells.

Fig. S3. NAC attenuated the Egt-mediated oxidative stress in CRC cells.

Fig. S4. Egt regulated sirtuins in normal and CRC cells.

Fig. S5. Egt outcome in CRC cell cycle.

Fig. S6. Egt effects on CRC cell death.

Fig. S7. Egt triggered ROS accumulation in CRC cells *via* SIRT3.